

Article

Utilization of Renewable Carbon in Electric Arc Furnace-Based Steel Production: Comparative Evaluation of Properties of Conventional and Non-Conventional Carbon-Bearing Sources

Lina Kieush ^{1,*} , Johannes Schenk ¹ , Andrii Koveria ² , Gerd Rantitsch ³ , Andrii Hrubciak ⁴  and Horst Hopfinger ⁵

¹ Department of Ferrous Metallurgy, Montanuniversitaet Leoben, 8700 Leoben, Austria

² Department of Chemistry, Dnipro University of Technology, 49005 Dnipro, Ukraine

³ Department of Geology and Economic Geology, Montanuniversitaet Leoben, 8700 Leoben, Austria

⁴ G.V. Kurdyumov Institute for Metal Physics of the National Academy of Sciences of Ukraine, 02000 Kyiv, Ukraine

⁵ Department of Ceramics, Montanuniversitaet Leoben, 8700 Leoben, Austria

* Correspondence: lina.kieush@unileoben.ac.at

Abstract: Conventional (anthracite, calcined petroleum coke, and coke) and non-conventional (biochar, and biocokes (3 wt.% torrefied wood, and 3 wt.% petroleum coke + 3 wt.% charcoal)) carbon-bearing sources have been studied for their use in electric arc furnace (EAF)-based steel production. Commonly, for the use of carbon sources in EAFs, one of the important properties is the content of fixed carbon, the release of volatiles as well as the elemental composition of inorganics. The properties of six carbon sources were analyzed by determining the proximate analysis, X-ray fluorescence analysis (XRF), coke reactivity index (CRI), and strength after reaction with CO₂ (CSR), Brunauer–Emmett–Teller (BET) specific surface area and Barrett–Joyner–Halenda (BJH) pore size and volume analysis, ash chemical analysis, optical and scanning microscopy, Raman spectroscopy and X-ray diffraction (XRD) analysis. The results indicate biocoke as a promising option to replace conventional carbon-bearing sources. In the sample set, the fixed carbon, volatiles, and ash content of the biocokes were similar despite the total difference in additives. Additionally, the use of additives did not significantly affect the biocoke reactivity indices, but slightly decreased the strength after the reaction with CO₂. Carbon-bearing sources have been characterized in terms of their structural properties. XRD analysis revealed that the amount of disordered carbon increased in the order: coke < calcined petroleum coke ~ biocoke (3 wt.% torrefied wood) < biocoke (3 wt.% petroleum coke + 3 wt.% charcoal) < biochar. The results obtained on the physical, chemical, and structural properties of carbon sources are the basis for further research on the behavior of slag foaming.

Keywords: coke; biochar; biocoke; calcined petroleum coke; EAF-based steel production



Citation: Kieush, L.; Schenk, J.; Koveria, A.; Rantitsch, G.; Hrubciak, A.; Hopfinger, H. Utilization of Renewable Carbon in Electric Arc Furnace-Based Steel Production: Comparative Evaluation of Properties of Conventional and Non-Conventional Carbon-Bearing Sources. *Metals* **2023**, *13*, 722. <https://doi.org/10.3390/met13040722>

Academic Editors: Chenguang Bai and Felix A. Lopez

Received: 29 January 2023

Revised: 3 March 2023

Accepted: 4 April 2023

Published: 6 April 2023



Copyright: © 2023 by the authors. Licensee MDPI, Basel, Switzerland. This article is an open access article distributed under the terms and conditions of the Creative Commons Attribution (CC BY) license (<https://creativecommons.org/licenses/by/4.0/>).

1. Introduction

Operating an electric arc furnace (EAF) is a well-established way of steel production [1–4]. EAF-based steel production accounts for approximately 26% [5,6] of the global output (~42% in the EU), according to the World Steel Association [7]. More than 40% of the energy in the current EAFs originates from natural gas and coal [8–10], corresponding to about 5 to 15 kg/t of liquid steel [11]. Usually, anthracite, coke (metallurgical or petroleum), or graphite is used as the source of carbon. Carbon-bearing sources are used as charged carbon (lumped within the basket), which consumes surplus oxygen during the melting stage and delivers heat or injected carbon, which interacts with oxygen to produce a foamy slag.

The operation with foamy slag enables higher productivity, a reduction in electrode consumption and arc noise reduction due to arc coverage, an increase in the average power due to improved arc stability, a reduction in the wall thermal stress, reduction in electric

energy consumption due to better thermal efficiency, lower nitrogen absorption, and a reduction in harmonic electric disturbances [12–15].

To achieve the foaming process, approximately 5–10 kg of injected carbon is used in an EAF [16]. The main requirements for carbon-bearing materials are a high carbon content (>85 wt.%, dry basis), a low ash content, and a bulk density of about 1000 kg/m³.

However, conventional carbon sources (anthracite, coke, or graphite) are responsible for 60–70% of direct greenhouse gas (GHG) emissions [8]. Looking for new ways to reduce CO₂ emissions [17] and achieve carbon neutrality and a circular economy [18,19], the partial or complete replacement of conventional carbon sources with materials such as biomass [20] or biochar has been investigated [16,21–27]. Carbon from biochar directly reacts with iron oxide (FeO) or reduces FeO indirectly through an intermediate gasification stage [28]. Notably, biochar usually contains a large amount of volatile matter (VM) including hydrogen [29]. Hydrogen contributes to the reaction of FeO to Fe and H₂O [30]. The indirect reaction of the water–gas conversion supports the gasification of solid carbon, accelerating the slag and carbon reaction. Hydrogen in the gas phase also increases the carbon gasification rate because H₂ and H₂O react faster with carbon and slag than CO and CO₂. In addition, FeO reacts faster with hydrogen compared to CO [16]. This provides the advantage of using biochar instead of anthracite [31] or coke, which is characterized by a small amount of VM and a relatively low amount of hydrogen [32–34]. In addition, for the scrap/EAF route, charcoal was assumed to replace the charge fully, injectant, and recarburizer carbon (85% C) in an EAF on an equivalent fixed carbon basis [35]. Partial or complete application of biomass/biochar is considered as a good option [36,37]. However, it is still a challenging issue in EAF-based steel production as the carbon source should have sufficient fixed carbon. Nevertheless, EAF-based steel production with biomass can reduce CO₂ emissions by 83% [38].

Shukla [39] demonstrated the thermo-chemical conversion of biomass to renewable fuels at a temperature below 1000 °C, which was lower than the steelmaking temperature of 1550–1650 °C. It was concluded that in the scrap-EAF route, biomass could be used as a slag foaming agent and in a cogeneration plant.

Demus et al. [22] assessed that biocoal from biogenic residues had great potential for industrial-scale EAF steelmaking. However, it was noticed that there were some problems in handling highly reactive carbonaceous materials with a high specific surface. Therefore, they suggested the use of biocoal briquettes.

Bianco et al. [40] characterized biochar from grape seed and wood residues, anthracite, and petroleum coke to study the slag foaming capability. It was concluded that petroleum coke had the highest carbon value of 93% and the lowest yield of VM of 1%. Biochar from the wood residues was characterized by the lowest carbon values and VM of 60% and 13.5%, respectively.

The thermochemical properties of two biochars obtained from the grape seed and pumpkin seed chars were studied by Fidalgo et al. [41] as an injected and/or charged carbon. They found that grape seed charcoal was more volatile and had a higher ash content than the charcoal and pumpkin seed charcoal. Thermogravimetric analysis indicated that grape seed charcoal had a higher reactivity for gasification, combustion, and slow release of VM, which may contribute to the supply of heat and sustaining reactions in the slag phase for a long time.

Kalde et al. [42] studied the reactivity and combustion behavior of wood produced by hydrothermal carburization (in the form of pellets), torrefaction (in the form of pellets), and pyrolysis as well as non-processed biomass such as palm kernel shells. Based on the obtained results, palm kernel shells were selected for a series of tests in an industrial-scale EAF. A study of reactivity as a function of time eliminated most materials due to a potentially explosive reaction that is possible when introduced into an industrial furnace. Based on the obtained results, palm kernel shells were selected for a series of tests on an industrial scale EAF.

Biochar produced by two different technologies (woody biomass after slow pyrolysis technology at 900 °C, and biochar from woody biomass after fast pyrolysis technology at 400 °C), graphite, coke, and char from tire pyrolysis were studied by Huang et al. [43]. Carbonaceous materials were characterized in terms of their chemical composition and carbon structure by Raman spectroscopy and XRD analysis. It was shown that materials were in the following microstructural order: graphite > coke > tire char > biochar from woody biomass after slow pyrolysis > biochar from woody biomass after fast pyrolysis technology at 400 °C. Moreover, it was found that the smooth surface of the biochar reduced the foaming of the slag. The interaction between biochar and slag was weak compared to other carbonaceous materials.

The reduction reactions and foaming of the slag in EAF depend not only on the physical and chemical properties of the slag but on the physicochemical properties of the carbon source. Indicators of proximate analysis, reactivity, micropores, and crystallinity show the physical and chemical properties of carbon sources and determine the kinetics of reactions with their participation. The most general indicator of the quality of carbon sources is reactivity, the value of which depends on the ordering of the carbon structure as well as on the proximate analysis indicators.

In this paper, anthracite, calcined petroleum coke, and high-temperature coke were studied as conventional carbon-bearing sources. Two types of biocoke and biochar were selected as alternative carbon-bearing sources. The specific objective was to study the physicochemical and microstructural properties of conventional and non-conventional carbon-bearing sources to assess the requirements of the carbon materials for EAF application.

2. Materials and Methods

2.1. Sample Materials

Calcined petroleum coke (CPC) with a grain size of 0–3 mm, a by-product of the oil refinery “MiRO” Germany, was provided by Stahl- und Walzwerk Marienhütte GmbH, Graz, Austria. The anthracite (Anth) sample with a grain size of 0–3 mm was taken from Vietnam; conventional coke (C) lumps as well as wood biochar pellets obtained at approximately 600 °C (Bch) were provided by Voestalpine Stahl GmbH, Linz, Austria. Samples of biocoke with 3 wt.% torrefied wood (BC1) and biocoke with 3 wt.% petroleum coke + 3 wt.% charcoal (BC2) were provided by ThyssenKrupp Steel Europe AG, Duisburg, Germany. It should be noted that the samples of biocoke were obtained in 2014 (BC2) and 2015 (BC1), which could have affected the quality of the biocokes. Low VM coal, medium VM coal, and high VM coal were used to prepare the base blends. The composition of the coal blends for BC1 and BC2 differed in additives to replace coals (Table 1).

Table 1. Composition of the blend for obtaining BC1 and BC2 (wt.%).

Blend Components	BC1	BC2
	Base Blend (LV + MV + HV) + 3 wt.% Torrefied Wood, Medium Temperature of 235–275 °C	Base Blend (LV + MV + HV) + 3 wt.% Petroleum Coke + 3 wt.% Charcoal
Low volatile (LV) coal	40	40
Medium volatile (MV) coal	30	29
High volatile (HV) coal	27	25
Petroleum coke	-	3
Charcoal	-	3
Torrefied wood (medium temperature of 235–275 °C)	3	-

The proximate and ultimate analyses for carbon-bearing sources (Table 2) were carried out according to ASTM D3172-13 [44]. The calorific value for the anthracite, coke, and biocoke samples (Table 2) was determined according to ISO 1928:2020 and biochar according to ISO 18125:2017 [45,46].

Table 2. Proximate and ultimate analyses of the carbon-bearing sources.

Carbon-Bearing Source	Proximate Analysis (wt.%)					Ultimate Analysis (wt.%)				Calorific Value (kJ/kg)
	M	VM (db)	VM (daf)	Ash (db)	S (db)	C (db)	H (db)	N (db)	C _{fix} (db)	
Anthracite	5.91	3.69	4.12	10.50	0.48	82.58	2.19	0.97	85.81	27.78
Calcined petroleum coke	0.17	0.44	0.45	0.93	0.63	97.26	0.29	1.49	98.63	32.74
Coke	2.27	1.42	1.59	10.82	0.77	90.56	0.30	1.05	87.76	29.47
Biochar	2.67	39.28	41.04	4.29	trace	72.74	4.62	0.24	56.43	26.87
Biocoke1	0.10	0.70	0.79	11.43	0.56	86.50	0.22	1.29	87.87	29.28
Biocoke2	0.10	0.30	0.34	11.54	0.61	86.40	0.18	1.41	88.16	29.30

M is moisture; C is carbon; H is hydrogen; N is nitrogen; S is sulfur; db is dry basis; daf is dry ash-free basis; VM(daf) = VM(db)·100/(100 – ash yield (db,%)); C_{fix}, wt.% = 100 – (wt.% VM (db) – wt.% Ash (db)).

2.2. Methods

The coke reactivity index (CRI) and coke strength after reaction with CO₂ (CSR) were determined according to ISO 18894:2018 [47]. Pre-dried coke weighing 200 ± 3 g with particle sizes from 19.0 to 22.4 mm was heated in a reaction vessel to a temperature of 1100 °C in a nitrogen atmosphere. Subsequently, the atmosphere was changed to carbon dioxide and held for 2 h. After that, the coke was cooled in a nitrogen atmosphere to 50 °C. Mass loss in the course of the CRI tests was recorded by a Mettler Toledo XP64000L balance. To determine the CSR, the reacted coke was treated in a tumbler (Model TB 5000 of R.B. Automazione, Genoa, Italy) for 600 revolutions in 30 min. After that, the coke was sieved, and the sample greater than 10.0 mm was weighed. All tests were repeated.

Before the combined test method of determining the Brunauer–Emmett–Teller (BET) specific surface area (SSA) and Barrett–Joyner–Halenda (BJH) pore size and pore volume, the samples were degassed for 3 h at a temperature of 300 °C and p/p₀ of 0.00–0.30. Degassing of anthracite and biochar was carried out for 24 h at a temperature of 120 °C and p/p₀ of 0.0001–0.99. The measurements were carried out at 77.3 K (–195.8 °C) using a Micromeritics Tristar II 3020 (Micromeritics, Norcross, GA, USA) instrument in a nitrogen atmosphere following ISO 9277:2010 [48]. The weight of the sample was 0.5 g with a grain size of <150 µm. All tests were repeated twice.

Images of the samples were obtained via optical microscopy Polyvar Reichert–Jung MEF 2 and Clemex Vision PE Software version 7.0. Samples were also observed via a scanning electron microscope SEM FEI Quanta 200 Mk² (FEI Technologies Inc., Oregon, OR, USA) equipped with an energy-dispersive (EDS) detector, back-scattered electron (BSE) detector, and a digital microscope Keyence VHX-E20 (Keyence, Itasca, IL, USA). After SEM/EDS analysis, the mineral matters were all normalized to 100 wt.%.

X-ray diffraction (XRD) spectra of the powdered samples were obtained using a Bruker AXS D8 (Bruker Corporation, Billerica, MA, USA) advance diffractometer with a lynxeye detector and a Cu X-ray tube with Cu K α radiation. The crystallite height (L_c), carbon crystallite width (L_a), and interlayer spacing between the aromatic planes of the carbon crystallites (d₀₀₂) were calculated using the Scherrer equation [49] and Bragg's Law [50]. The crystalline stacking layer number N was calculated by an equation with the parameters d₀₀₂ and L_c according to [51].

A Horiba Labram HR Evolution instrument (Horiba, Ltd., Kyoto, Japan), equipped with a 100 mW Nd: Yag (532 nm) laser, a confocal microscope (hole aperture = 100 µm), an 1800 g/mm grating, and a Peltier cooled CCD detector were used to obtain Raman spectra as they can confidently characterize the microstructural state of the carbon materials [52].

To assess the microstructural variability of the experimental samples within a sample, a lump of each sample ranging in size from 19.0 to 22.4 mm was examined by analyzing 10 random spots (diameter of ca. 1.6 μm) per lump on a section through the lump using a 10 \times objective and laser energy of 100 mW.

X-ray fluorescence analysis (XRF) was conducted to determine the ash chemical composition of all samples according to ASTM D4326-21 [53]. The mass fraction (%) of chemical elements was measured using an energy-dispersive analyzer EXPERT 3L. The detection limits of the elements ranged from 1 to 10 ppm. The resolution of the detector (for $K\alpha\text{Mn}$) at nominal load did not exceed 149 eV.

3. Results

Samples of anthracite, calcined petroleum coke, conventional coke, and two samples of biocoke were characterized by a major amount of silica and aluminum oxide (Table 3). Iron, calcium oxide, and potassium oxide were present in smaller amounts. The biochar sample was characterized by a significant amount of calcium oxide, chlorine, and a much smaller amount of silica than the other carbon-bearing sources. Phosphorus oxide was present in small amounts in the coke (0.07 wt.% db) and biochar (0.08 wt.% db) samples. The difference in the content of phosphorus oxide was not large between the biocoke samples and amounted to 0.41 wt.% db (BC1) and 0.34 wt.% db (BC2).

Table 3. The XRF results of ash composition of carbon-bearing sources (wt.% db).

Ash Composition	Carbon-Bearing Source					
	Anthracite	Calcined Petroleum Coke	Coke	Biochar	Biocoke1	Biocoke2
Fe	4.59	2.60	4.68	6.31	3.11	3.24
SiO ₂	52.73	56.63	52.67	5.30	59.10	60.20
Al ₂ O ₃	31.26	13.57	30.79	n.d.	29.90	28.20
MgO	n.d.	n.d.	n.d.	10.96	0.47	0.75
CaO	2.18	3.15	2.21	53.77	1.17	1.56
TiO ₂	1.58	1.04	1.62	0.39	1.60	1.51
K ₂ O	4.34	15.54	4.57	n.d.	1.31	1.51
P ₂ O ₅	0.56	0.31	0.07	0.08	0.41	0.34
MnO	0.05	0.39	0.05	3.36	0.05	0.05
NiO	n.d.	n.d.	n.d.	n.d.	0.02	0.02
Ni ₂ O ₃	0.02	0.75	0.02	0.04	n.d.	n.d.
Ash basicity (B1)	0.04	0.06	0.04	10.15	0.02	0.03

n.d., not detected; minor components were excluded.

The BC1 CRI value was lower than the CRI of BC2 and had 29.18 and 32.50 wt.%, respectively (Table 4), being much lower compared to conventional coke.

The lowest value of BET SSA was characterized by anthracite (0.71 m²/g). A sample of calcined petroleum coke was also characterized by a small BET SSA value of 0.95 m²/g. The conventional coke sample had a BET SSA of 2.54 m²/g. The BET SSA for BC1 was higher than that for BC2 and had values of 4.85 and 4.20 m²/g, respectively. Biochar was characterized by the highest BET SSA value of 42.95 m²/g.

Table 4. The quality properties of carbon-bearing sources.

Carbon-Bearing Source	Quality Properties						
	CRI (wt.%)	Std	CSR (wt.%)	Std	BET N ₂ -Specific Surface Area (m ² /g)	BJH Adsorption Cumulative Surface Area of Pores (cm ³ /g)	BJH Adsorption Average Pore Width (4 V/A), (Å)
Anthracite	n.a.	n.a.	n.a.	n.a.	0.71	0.000583	58.205
Calcined petroleum coke	n.a.	n.a.	n.a.	n.a.	0.95	0.001434	67.439
Coke	31.68	1.31	62.87	0.94	2.54	0.002297	49.054
Biochar	n.a.	n.a.	n.a.	n.a.	42.95	0.004594	30.127
Biocoke1	29.18	1.70	52.89	0.79	4.85	0.000958	85.853
Biocoke2	32.50	1.13	50.95	0.21	4.20	0.002406	44.102

n.a., not available; std, standard deviation.

3.1. Optical Microscopy and SEM Analysis

The SEM images of anthracite showed lumped particles up to 3 mm in size, which were used as injected carbon in the EAF (Figure 1). During the study, the presence of mechanical inorganic contaminations on the surface of the particles was noticed.

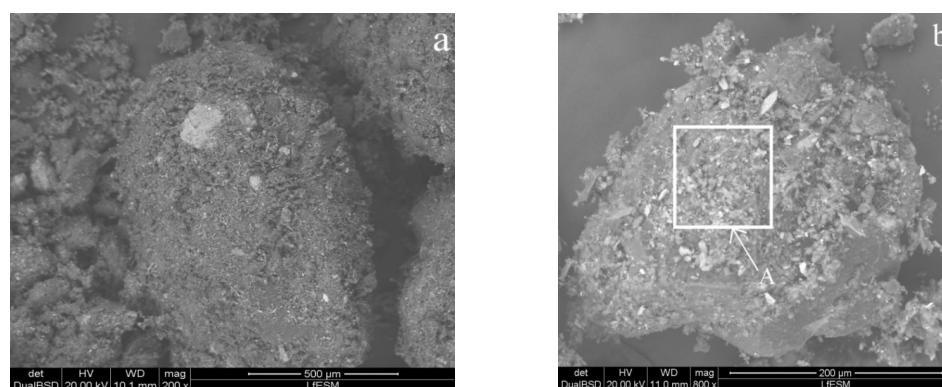


Figure 1. (a) SEM image of the anthracite particles, magnification 200×. (b) SEM image of anthracite particle with a spot of the EDS spectrum (A), magnification 800×.

The surface of the particles of the calcined petroleum coke sample was smooth, flaky, and cracked, as shown in Figure 2b.

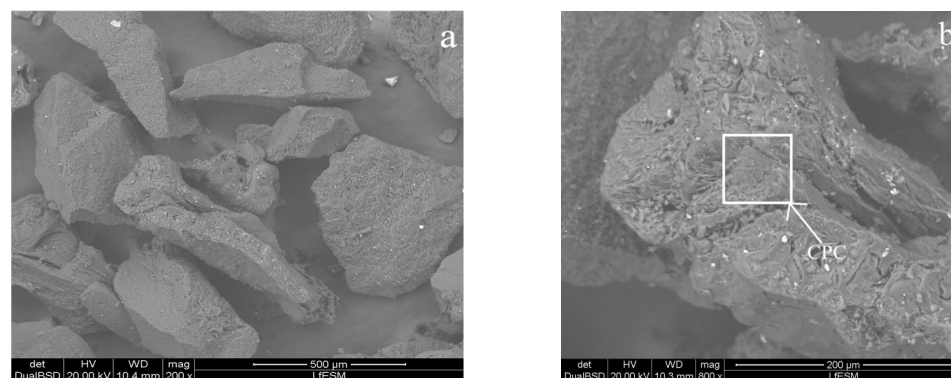


Figure 2. (a) SEM image of the calcined petroleum coke sample, magnification 200×; (b) SEM image of the calcined petroleum coke sample with a spot of the EDS spectrum (CPC), magnification 800×.

Biochar particles were the most porous material (Figure 3), which was confirmed by the highest BET SSA value (see Table 4). The coke sample was a porous-fractured material consisting of pores, microcracks, and a hard carbon matrix with organic and inorganic inclusions (Figure 4b). It is evident from Figure 4b that this was a heterogeneous material composed of organic carbon, mineral substances, and many pores. The microstructures of BC1 (Figure 5a,b) and BC2 (Figure 5c,d) did not differ significantly. These were visually characterized by the presence of large pores, unlike the conventional coke presented in Figure 4a,b.

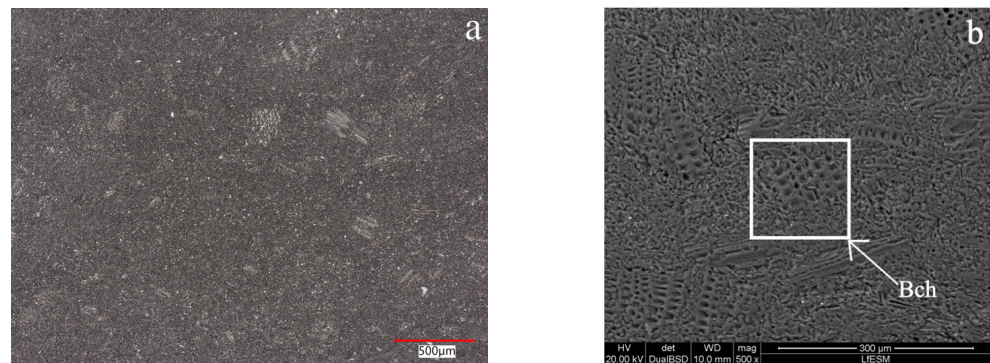


Figure 3. Images of the biochar sample. (a) Optical image of the biochar sample, magnification 100×. (b) SEM image of the biochar sample with a spot of the EDS spectrum (Bch), magnification 500×.

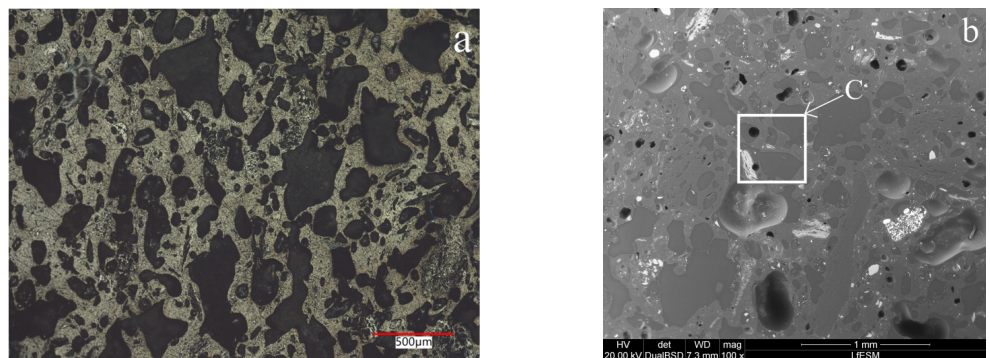


Figure 4. Images of the coke sample. (a) Optical image of the coke sample, magnification 100×; (b) SEM image of the coke sample with a spot of the EDS spectrum (C), magnification 100×.

Si, Al, Mg, Ca, and Fe-oxides were found in all samples (Table 5). The predominant presence of alumina-silicates characterized the coke and anthracite samples. Potassium was also detected for all specimens, with the highest value for calcined petroleum coke. Sulfur was only detected in the anthracite sample. The biocoke samples did not differ in the presence of elements such as Al, Si, Ca, and Fe.

3.2. X-ray Diffraction Analysis

The lattice distance d_{002} for anthracite, calcined petroleum coke, coke, and BC1 was 0.35 nm and 0.37 nm for BC2, which was slightly higher (Table 6). Biochar was characterized by the highest value of d_{002} (0.45 nm). The largest value of the carbon crystallite height was characterized by anthracite (2.08 nm) followed by coke (1.86 nm), and the lowest by biochar (0.69 nm). The number of the crystal stacking layers was larger (6.94) in anthracite than in the other four coke samples.

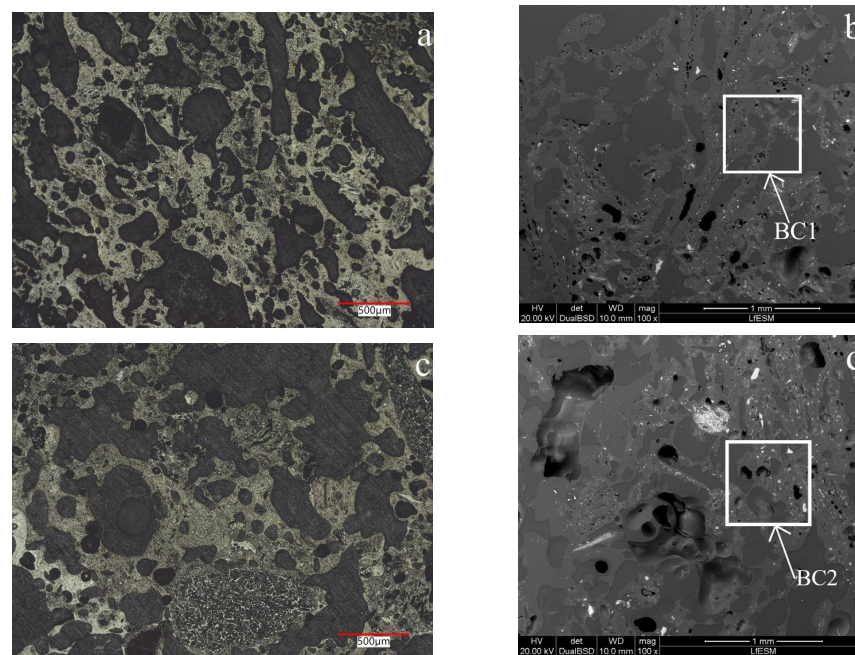


Figure 5. Microscopic images of the biocoke samples. (a) Optical image of the biocoke1 sample, magnification 100×. (b) SEM image of the biocoke1 sample with a spot of the EDS spectrum (BC1), magnification 100×. (c) Optical image of the biocoke2 sample, magnification 100×. (d) SEM image of the biocoke2 sample with a spot of the EDS spectrum (BC2), magnification 100×. The arrow indicates the spot for which the EDS was applicable.

Table 5. The SEM/EDS analysis results for the carbon-bearing sources.

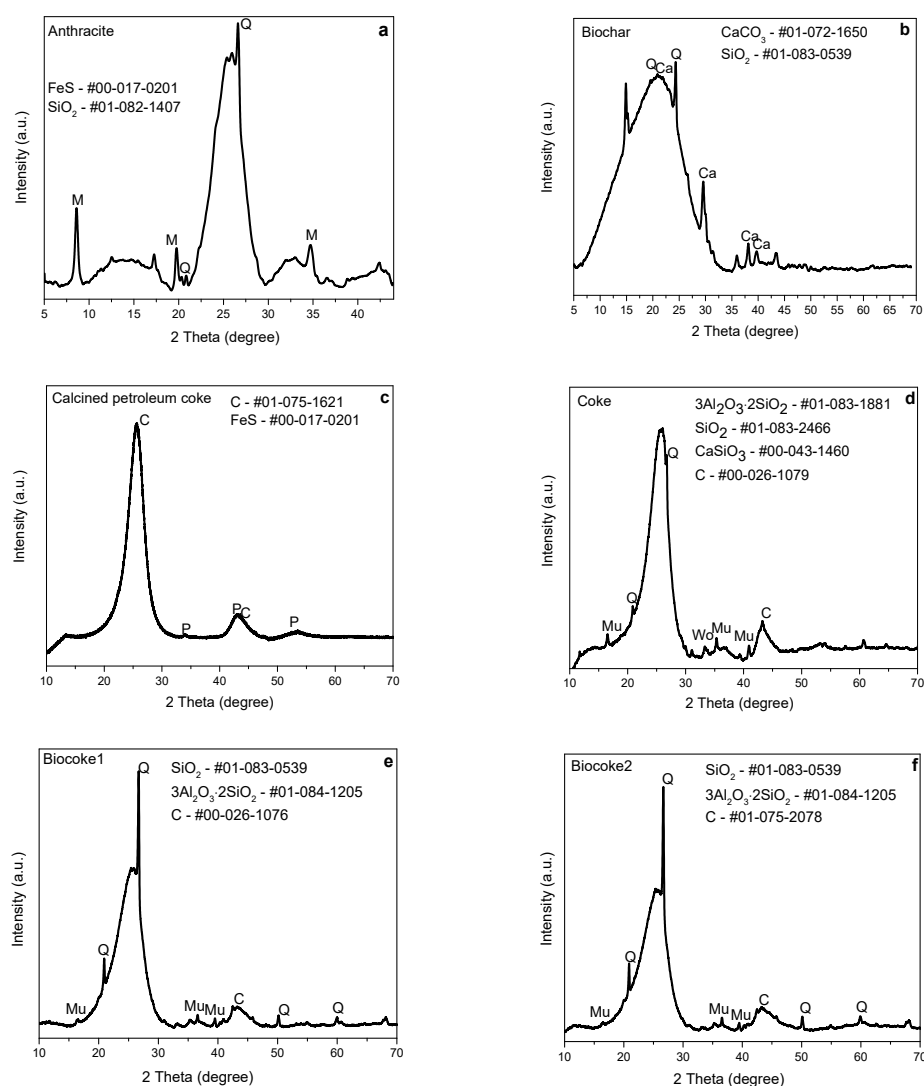
Chemical Composition, wt.%	Carbon-Bearing Source					
	Anthracite	Calcined Petroleum Coke	Biochar	Coke	Biocoke1	Biocoke2
O	38.51	44.49	25.66	35.42	36.73	46.73
Na	n.d.	n.d.	1.18	1.48	0.26	0.73
Mg	0.69	1.42	0.19	0.27	0.05	0.16
Al	21.61	7.18	0.54	23.23	23.58	23.37
Si	27.56	26.47	1.45	27.19	25.56	25.65
S	0.92	n.d.	n.d.	n.d.	n.d.	n.d.
K	4.77	12.90	1.01	1.58	0.16	2.35
Ca	0.50	2.25	0.65	7.06	0.16	0.14
Ti	n.d.	0.60	n.d.	0.20	0.03	0.05
Cr	n.d.	0.90	1.04	0.12	0.01	n.d.
Mn	n.d.	0.30	n.d.	n.d.	1.30	n.d.
Fe	4.37	2.60	6.32	3.11	5.25	5.45
Ni	n.d.	0.53	2.77	0.11	0.06	0.03
Cu	1.06	0.02	0.04	0.12	n.d.	n.d.

n.d., not detected; minor components were excluded.

In the anthracite sample (Figure 6a), quartz and muscovite [31] were found. In the biochar, quartz and calcite (Figure 6b) were identified. Quartz and pyrite were found for calcined petroleum coke (Figure 6c). In addition, a weak peak at approximately $43^{\circ}2\theta$ was detected in the coke, BC1, and BC2 samples and assigned to graphite (Figure 6d–f). For coke, BC1, and BC2 (Figure 6e,f), the peak around $16.0^{\circ}2\theta$ was specified as mullite ($3\text{Al}_2\text{O}_3 \cdot 2\text{SiO}_2$), showing that the predominant crystalline phases were quartz and mullite.

Table 6. The XRD parameters for the carbon-bearing sources.

Carbon-Bearing Source	d_{002} , nm	L_c , nm	L_a , nm	N
Anthracite	0.35	2.08	1.64	6.94
Calcined petroleum coke	0.35	1.58	2.76	5.51
Biochar	0.45	0.69	1.16	2.53
Coke	0.35	1.86	3.69	6.31
Biocoke1	0.35	1.56	2.80	5.46
Biocoke2	0.37	1.32	2.08	4.57

**Figure 6.** The XRD spectra of mineral matter of carbon-bearing sources: (a) anthracite; (b) biochar; (c) calcined petroleum coke; (d) coke; (e) biocoke1; and (f) biocoke2. Q is quartz, M is muscovite, Ca is calcite, C is graphite, P is pyrite, Mu is mullite, and Wo is wollastonite.

The minerals of the cokes were not significantly different, but wollastonite (CaSiO₃) was also found in the coke [54]. Additionally, a weak peak was observed at approximately 43°2θ and was assigned to the (101) plane reflection of graphite.

3.3. Raman Spectroscopy

Carbon-bearing sources were characterized by the D-STA [55] parameter describing the microstructural order (the lower the parameter value, the better the level of microstructure order [52]). The lowest value of the D-STA for carbonized carbon sources corresponded to coke (Table 7). Furthermore, the most ordered carbon-bearing source was calcined petroleum coke. If two samples of biocokes were compared, then the lowest value of the D-STA corresponded to BC1. Biochar had the highest D-STA value, and consequently, the worst order of the microstructure.

Table 7. Raman spectral parameters (see [50]) (median of 10 spot measurements) for the carbon-bearing sources.

Carbon-Bearing Source	D-STA (Mean)	Std	G-STA (Mean)	Std	G Shape Factor (Mean)	Std	Dmax Position (Mean)	Std	Gmax Position (Mean)	Std	Dmax/Gmax-Ratio (Mean)	Std
Anthracite	166.4	0.2	133.1	0.4	1.4	0.0	1325.6	0.0	1600.0	0.0	0.8	0.0
Biochar	272.4	0.2	192.2	0.6	1.4	0.0	1352.3	0.0	1591.9	0.0	0.7	0.0
Calcined petroleum coke	219.8	0.1	204.6	0.2	1.3	0.0	1351.4	0.0	1586.7	0.0	0.9	0.0
Coke	197.0	0.2	210.3	0.1	1.2	0.0	1347.9	0.0	1593.8	0.0	1.1	0.0
Biocoke1	223.1	0.1	215.1	0.1	1.5	0.0	1351.5	0.0	1593.7	0.0	1.0	0.0
Biocoke2	248.9	0.6	233.1	0.2	1.2	0.0	1361.1	0.0	1593.4	0.0	0.9	0.0

Std, standard deviation.

Based on the results shown in Figure 7, a statistically significant structural difference in the D-STA parameter was seen between the samples of coke and calcined petroleum coke, coke and biochar, and between the samples of BC1 and BC2.

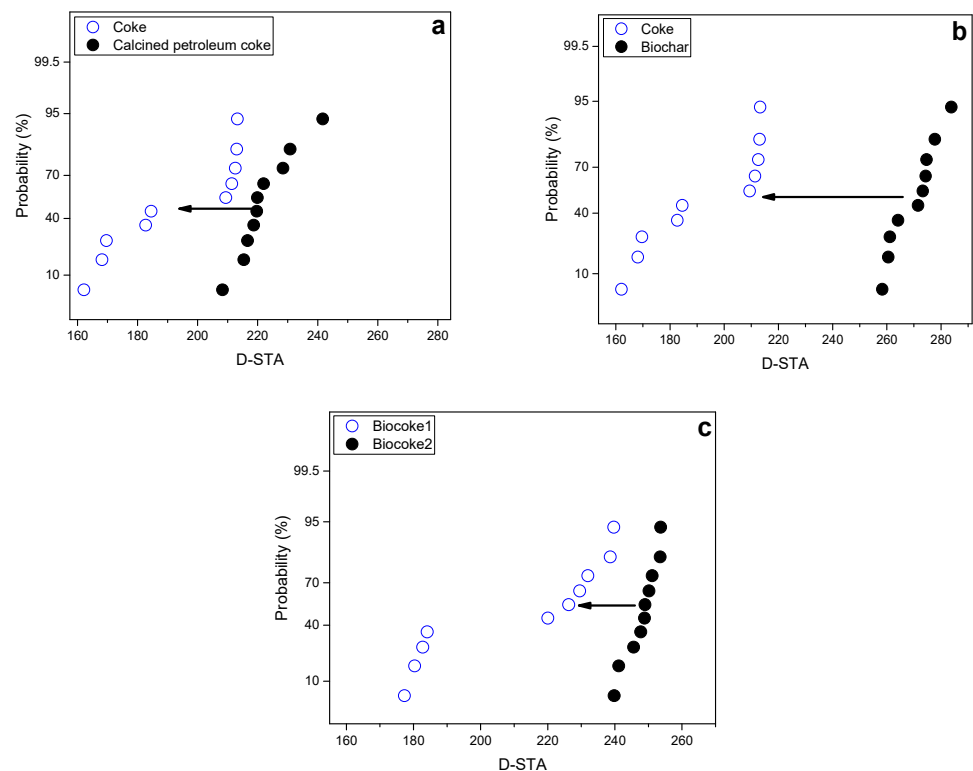


Figure 7. (a) Probability distribution of the D-STA parameter of coke and calcined petroleum coke; (b) coke and biochar; and (c) biocoke samples. The arrow indicates a statistically significant difference.

4. Discussion

The yield of VM of the carbonized carbon materials depends on the processing conditions. It is important to assess the difference in VM yield for biocokes in relation to the other indicators. The highest yield of VM was characterized as biochar (Table 2). The low ash content of calcined petroleum coke can be explained by the low mineral content of oil and heavy oil residues from oil refining that have been coked. The sulfur content was close to that of other materials. The high ash content of biocoke relative to other materials was due to the high mineral content of the blended coal components. The ash content and VM yield of the studied carbon-bearing sources determined the fixed carbon values. The elemental composition of materials subjected to carbonization depends on the temperature and the initial ratio of the main organic components of coal, oil, and biomass. Calcined petroleum coke had the lowest ash content and the highest carbon content, followed by coke and biocoke. Biochar had the lowest carbon content, with the highest hydrogen content simultaneously. The elemental composition, ash content, and moisture determined the calorific value. Obviously, calcined petroleum coke was characterized by the highest calorific value. Conventional coke and biocokes have similar values, exceeding anthracite and biochar.

A high fixed carbon value is essential for EAF steel production [35]. Therefore, coke is used as a source of injection carbon as well as calcined petroleum coke and anthracite. However, a high ash content of anthracite and coke (Table 2) excludes their recarburization, so calcined petroleum coke is therefore preferred. However, calcined petroleum coke, in turn, is a more limited and expensive carbon material than the other studied sources. Biochar has the advantage of a low ash content and practically does not contain sulfur as well as a high amount of hydrogen compared to conventional ones. However, its use is limited as it does not have sufficient fixed carbon (Table 2). Biocoke (torrefied wood/petroleum coke + charcoal is an alternative source for substituting conventional carbon sources) has enough fixed carbon for use in EAF steel production. However, biocoke is also characterized by a high ash content, and can therefore be proposed for use as a source of injection carbon.

One of the essential parameters for using carbon-bearing sources in EAF is the amount and nature of the minerals, as they potentially have an influence on this process (Cl and K) and on the steel properties (P) [26]. In the case of K and Cl, their presence can cause corrosion issues in the flue gas section of the EAF. Table 3 shows no significant difference in the ash composition of biocokes. However, BC2 was characterized by a lower content of phosphorus oxide. The lower value of phosphorus oxide for BC2 can be explained by the replacement of a large amount of less phosphorus-containing additives than in the components of the coal blend. The highest ash basicity was for biochar and was determined by the presence of CaO. The low content of CaO in biocokes can be explained by the low content of CaO in the coal blend and the slight influence on the change in CaO from the addition of biomaterials. The other samples had similar small values. The SEM/EDS analysis revealed that typical ash minerals were found in all samples [43,56,57].

The effect of the additive in the biocoke samples did not significantly influence the CRI (Table 4), as also observed by [58]. However, the CSR was influenced negatively. A low microstructural ordering might explain the lower CSR values due to an inert additive (3 wt.% torrefied biomass in the case of BC2). CSR was even lower for BC2 than for BC1, reflecting the overall higher amount of additives (3 wt.% charcoal and 3 wt.% petroleum coke) due to the fact that petroleum coke can be considered an inert additive.

The BET SSA of carbon sources is important since the process of interaction first begins along the surface. In addition, high BET SSA values indicate a high porosity of materials, which leads to an increase in the reactivity [40] of carbon sources, all other things being equal (chemical and structural properties). A mesopore structure characterized all of the studied samples according to the International Union of Pure and Applied Chemistry (IUPAC) definition (Table 4). Biochar was characterized by the greatest BET SSA value. It is

worth noting that the addition of 3 wt.% charcoal and 3 wt.% petroleum coke into BC2 did not significantly affect the BET SSA compared to BC1 with 3 wt.% torrefied biomass.

Although d_{002} for the four coke samples was approximately the same (Table 6), the value of L_c was higher for coke. When comparing the BC1 and BC2 samples, 6 wt.% of total additives in BC2 had more effect on the degree of graphitization compared to the sample with 3 wt.% of total additives in BC1. As the XRD analysis results showed, after coking the blend to obtain BC1, the best ordering of the structure was observed compared to BC2. Additional confirmation was the lower CRI value, which was consistent with the results in Table 4. In addition, it was noticed that anthracite had a more ordered carbon structure and larger crystallite size compared to carbon sources that had been artificially ordered by carbonization. Similar results and conclusions regarding the microstructural ordering of anthracite and coke have been shown in [59,60].

It can be summarized that the amount of disordered carbon structure increases in the following order: C < CPC ~ BC1 < BC2 < Bch (Figure 8) excluding anthracite, as it is a naturally ordered carbon material compared to the other four samples subjected to carbonization.

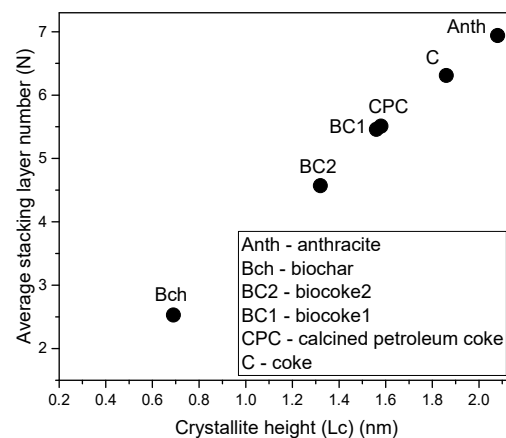


Figure 8. Relationship between the crystallite height (L_c) and crystalline stacking layer number (N).

As can be seen from the results above, conventional high-temperature coke is a more ordered material than other studied materials ordered by carbonization (Table 7). When comparing the microstructural ordering between BC1 and BC2, in BC1, the total amount of the additive is a more ordered carbon material, which is consistent with the results of the XRD analysis.

According to Figure 9a, the higher the L_c , the lower the D-STA value, which characterizes the carbon material as more ordered, and this relationship showed the order: Bch < BC2 < BC1 ~ CPC < C. Figure 9b shows the relationship between L_c and the D_{max}/G_{max} ratio (mean). The D_{max}/G_{max} ratio increased in the order of C > BC1 > CPC = BC2 > Bch, indicating increasingly growing aromatic layers that develop a local molecular orientation.

It can be summarized that the carbonization of biochar is an essential condition to improve its properties and the possibility of its further use. Regarding ordering, the biocoke samples were less ordered materials than coke and calcined petroleum coke.

Generally, coke is the most common metallurgical carbon source. However, for EAFs, coke is used, which is obtained according to the requirements of the BF process, namely with low reactivity and high strength.

During the smelting process, the carbon source should have certain reactivity, which can be on the same level as conventional carbon sources or those more reactive. Therefore, the use of biocoke for EAFs can have a number of advantages, namely, increased reactivity, reduced ash content (due to lower ash content of biomaterials), sulfur content, high strength, and reduced GHG emissions with other indicators that are not inferior to conventional

coke (for instance, volatile matter, fixed carbon). In the case of using coke for EAFs, quality characteristics more suitable for BF production than for EAF have to be considered.

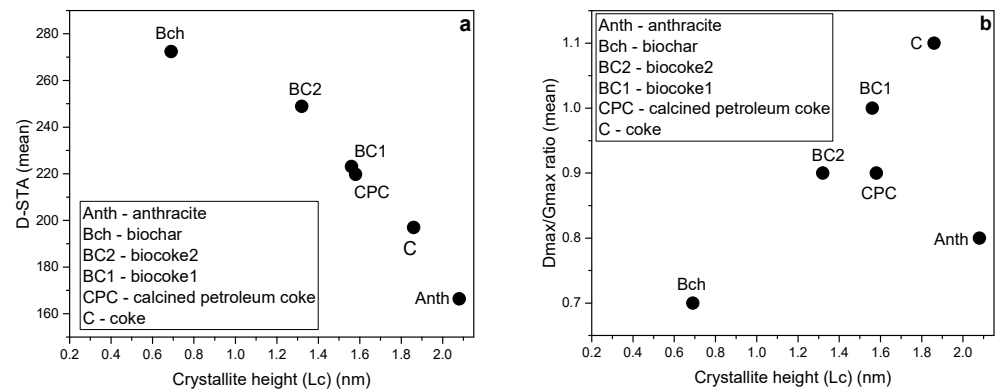


Figure 9. Relationship between the parameters of crystallite height (L_c) and selected Raman parameters. (a) Relationship between crystallite height (L_c) and D-StA (mean). (b) Relationship between crystallite height (L_c) and the Dmax/Gmax ratio (mean).

Thus, biocoke can be considered as a promising option to replace conventional carbon sources since biomass/charcoal additives have less effect on changing the properties of coke while reducing the ash content and sulfur content, and the volatile matter can be on a level with conventional coke since this parameter depends on the severity of carbonization. In the case of biocoke, achieving high values of fixed carbon content at the same level as coke is possible. It has been established that up to 5 wt.% bio-additives can be used to replace coal in the production of biocoke without a significant deterioration in the reactivity [61]. Compared to biochar, it is a less reactive and more mechanically strong material.

5. Conclusions

A comparative study investigated the properties (CRI and CSR, BET SSA, BJH pore size and volume, ash chemical composition, microstructure) of conventional and non-conventional carbon-bearing sources. Characteristics of the crystallinity of carbon sources obtained using Raman spectroscopy and XRD analysis can be of scientific and practical interest as the ordering of carbon sources determines their interaction with oxygen to create slag foam and further influence the smelting process in EAF. The obtained results assessed the suitability of different carbon-bearing sources for their use in EAF-based steel production. The following conclusions can be drawn for conventional carbon-bearing sources:

- (1) The use of studied anthracite has the advantage of being characterized by a relatively low sulfur value of 0.48 wt.% and a rather high fixed carbon value of 85.81 wt.%. However, it was characterized by an ash value of 10.50 wt.%. The disadvantages of anthracite for use in the EAFs are less fixed carbon compared to carbonized materials as well as a lower calorific value.
- (2) Using calcined petroleum coke as a carbon source has low ash and VM content advantages. In contrast, the sulfur content was similar to other carbon-bearing materials (except biochar). Calcined petroleum coke had the highest fixed carbon content of 98.63 wt.% and calorific value of 32.74 wt.% compared to other conventional and non-conventional carbon-bearing sources. As a result of calcination, petroleum coke was characterized by a layered and cracked structure. This material had the highest potassium content compared to the other studied materials. Calcined petroleum coke had a well-ordered microstructure, predominantly inferior to coke.
- (3) The use of coke was determined by low values of VM and sulfur as well as high values of fixed carbon and calorific value. The ash composition of coke was predominantly characterized by silica and aluminum oxide. CRI and CSR were within the requirements. In terms of microstructural ordering, coke was characterized by

the least amount of disordered carbon structure and had the best ordering among artificially ordered materials after carbonization.

The following conclusions were drawn for non-conventional carbon-bearing sources:

- (1) The use of biochar is preferred over conventional carbon-bearing sources since it is characterized by a low ash content, practically no sulfur, and a high hydrogen content. However, a low fixed carbon value limits its use. Biochar was also characterized by the highest ash basicity value and had the highest BET SSA value. Biochar also had an inferior microstructural order. Consequently, carbonization at 600 °C or higher is necessary for its use to maintain the required fixed carbon value and reduce VM.
- (2) Biocoke is a good option to replace conventional carbon-bearing sources. Both biocoke samples had high fixed carbon values but slightly higher ash values. The CSR values were much lower, which could be explained by the influence of inert additives. The biocoke samples were inferior to conventional carbon sources obtained after carbonization in terms of ordering. Nevertheless, using biocoke for EAFs can have benefits such as increased reactivity, reduced ash content (due to lower ash content of biomaterials) and sulfur content, high strength, and reduced GHG emissions.

Author Contributions: Conceptualization, L.K. and J.S.; Investigation, L.K., A.H. and H.H.; Methodology, L.K., A.K. and A.H.; Supervision, J.S.; Writing—original draft, L.K.; Writing—review & editing, J.S., A.K. and G.R. All authors have read and agreed to the published version of the manuscript.

Funding: This research received no external funding.

Institutional Review Board Statement: Not applicable.

Informed Consent Statement: Not applicable.

Data Availability Statement: Not applicable.

Acknowledgments: This research was supported by the scholarship program “Scholarship of the Scholarship Foundation of the Republic of Austria, Postdocs,” [MPC-2022-02241], financed by the Federal Ministry of Education, Science and Research of Austria, which is gratefully acknowledged. Stahl-und Walzwerk Marienhütte GmbH, Graz, Austria; Voestalpine Stahl GmbH, Linz, Austria; and ThyssenKrupp Steel Europe AG, Duisburg, Germany are gratefully acknowledged for providing the sample materials for this research. The authors are also grateful to the reviewers for their insightful comments and efforts in improving the manuscript.

Conflicts of Interest: The authors declare no conflict of interest.

References

1. European Steel Technology Platform (ESTEP): Clean Steel Partnership Roadmap; 2020. Available online: <https://www.estep.eu/assets/Uploads/CSP-SRIA-Oct2021-clean.pdf> (accessed on 27 January 2023).
2. Suer, J.; Traverso, M.; Ahrenhold, F. Carbon Footprint of Scenarios towards Climate-Neutral Steel According to ISO 14067. *J. Clean. Prod.* **2021**, *318*, 128588. [CrossRef]
3. Reimann, A.; Hay, T.; Echterhof, T.; Kirschen, M.; Pfeifer, H. Application and Evaluation of Mathematical Models for Prediction of the Electric Energy Demand Using Plant Data of Five Industrial-Size EAFs. *Metals* **2021**, *11*, 1348. [CrossRef]
4. Schubert, C.; Büschgens, D.; Eickhoff, M.; Echterhof, T.; Pfeifer, H. Development of a Fast Modeling Approach for the Prediction of Scrap Preheating in Continuously Charged Metallurgical Recycling Processes. *Metals* **2021**, *11*, 1280. [CrossRef]
5. Suer, J.; Ahrenhold, F.; Traverso, M. Carbon Footprint and Energy Transformation Analysis of Steel Produced via a Direct Reduction Plant with an Integrated Electric Melting Unit. *J. Sustain. Metall.* **2022**, *8*, 1532–1545. [CrossRef]
6. Fan, Z.; Friedmann, S.J. Low-Carbon Production of Iron and Steel: Technology Options, Economic Assessment, and Policy. *Joule* **2021**, *5*, 829–862. [CrossRef]
7. Steel Statistical Yearbook 2019. Available online: <https://worldsteel.org/wp-content/uploads/Steel-Statistical-Yearbook-2019-concise-version.pdf> (accessed on 27 January 2023).
8. Cardarelli, A.; De Santis, M.; Cirilli, F.; Barbanera, M. Computational Fluid Dynamics Analysis of Biochar Combustion in a Simulated Ironmaking Electric Arc Furnace. *Fuel* **2022**, *328*, 125267. [CrossRef]
9. Kieush, L.; Koveria, A.; Schenk, J.; Rysbekov, K.; Lozynskiy, V.; Zheng, H.; Matayev, A. Investigation into the Effect of Multi-Component Coal Blends on Properties of Metallurgical Coke via Petrographic Analysis under Industrial Conditions. *Sustainability* **2022**, *14*, 9947. [CrossRef]

10. Mombelli, D.; Quadrio, M.; Mapelli, C.; Echterhof, T.; Fernandez Aparicio, L.; Sorger, C.; Griessacher, T.; Mudersbach, D.; Schüler, S. Influence of the Recirculation of Various By-Products Generated through Electric Arc Furnace Route on EAF Slag Quality. *ISIJ Int.* **2022**, *62*, 2610–2621. [CrossRef]
11. International Iron and Steel Institute. *EAF Technology. State of the Art & Future Trends*; IISI: Brussels, Belgium, 2000.
12. Ji, F.-Z.; Barati, M.; Coley, K.; Irons, G.A. Kinetics of coal injection into iron oxide containing slags. *Can. Metall. Q.* **2005**, *44*, 85–94. [CrossRef]
13. Coley, K.S. Progress in the Kinetics of Slag-Metal-Gas Reactions, Past Present and Future. *J. Min. Met. B Met.* **2013**, *49*, 191–199. [CrossRef]
14. Agnihotri, A.; Singh, P.K.; Singh, D.; Gupta, M. Foamy Slag Practice to Enhance the Energy Efficiency of Electric Arc Furnace: An Industrial Scale Validation. *Mater. Today Proc.* **2021**, *46*, 1537–1542. [CrossRef]
15. Menad, N.-E.; Kana, N.; Seron, A.; Kanari, N. New EAF Slag Characterization Methodology for Strategic Metal Recovery. *Materials* **2021**, *14*, 1513. [CrossRef]
16. Echterhof, T. Review on the Use of Alternative Carbon Sources in EAF Steelmaking. *Metals* **2021**, *11*, 222. [CrossRef]
17. Schmitz, N.; Sankowski, L.; Kaiser, F.; Schwotzer, C.; Echterhof, T.; Pfeifer, H. Towards CO₂-Neutral Process Heat Generation for Continuous Reheating Furnaces in Steel Hot Rolling Mills—A Case Study. *Energy* **2021**, *224*, 120155. [CrossRef]
18. Fit for 55 2022. Available online: <https://www.consilium.europa.eu/en/policies/green-deal/fit-for-55-the-eu-plan-for-a-green-transition/> (accessed on 27 January 2023).
19. Huang, D.; Dinga, C.D.; Tao, Y.; Wen, Z.; Wang, Y. Multi-Objective Optimization of Energy Conservation and Emission Reduction in China's Iron and Steel Industry Based on Dimensionality Reduction. *J. Clean. Prod.* **2022**, *368*, 133131. [CrossRef]
20. Wang, R.; Zhao, Y.; Babich, A.; Senk, D.; Fan, X. Comprehensive Study on the Reduction of Biomass Embedded Self-Reducing Pellets (SRP) under H₂ Involved Conditions by TG-DTA. *Powder Technol.* **2022**, *407*, 117654. [CrossRef]
21. Oliveira, T.L.; Assis, P.S.; Leal, E.M.; Ilídio, J.R. Study of Biomass Applied to a Cogeneration System: A Steelmaking Industry Case. *Appl. Therm. Eng.* **2015**, *80*, 269–278. [CrossRef]
22. Demus, T.; Echterhof, T.; Pfeifer, H.; Schulten, M.; Noel, Y.; Quicker, P. Investigations on the Use of Biogenic Residues as a Substitute for Fossil Coal in the EAF Steelmaking Process. In Proceedings of the 10th European Electric Steelmaking Conference, Graz, Austria, 25–28 September 2012; Volume 10.
23. Rejda, M.; Wojtaszek-Kalaizidi, M.; Gałko, G.; Mertas, B.; Radko, T.; Baron, R.; Książek, M.; Yngve Larsen, S.; Sajdak, M.; Kalaizidis, S. A Study on Bio-Coke Production—The Influence of Bio-Components Addition on Coke-Making Blend Properties. *Energies* **2022**, *15*, 6847. [CrossRef]
24. Demus, T.; Reichel, T.; Schulten, M.; Echterhof, T.; Pfeifer, H. Increasing the Sustainability of Steel Production in the Electric Arc Furnace by Substituting Fossil Coal with Biochar Agglomerates. *Ironmak. Steelmak.* **2016**, *43*, 564–570. [CrossRef]
25. Meier, T.; Hay, T.; Echterhof, T.; Pfeifer, H.; Rekersdrees, T.; Schlinge, L.; Elsabagh, S.; Schliephake, H. Process Modeling and Simulation of Biochar Usage in an Electric Arc Furnace as a Substitute for Fossil Coal. *Steel Res. Int.* **2017**, *88*, 1600458. [CrossRef]
26. Funke, A.; Demus, T.; Willms, T.; Schenke, L.; Echterhof, T.; Niebel, A.; Pfeifer, H.; Dahmen, N. Application of Fast Pyrolysis Char in an Electric Arc Furnace. *Fuel Process. Technol.* **2018**, *174*, 61–68. [CrossRef]
27. Firsbach, F.; Senk, D.; Babich, A. Multi-Step Recycling of BF Slag Heat via Biomass for CO₂ Mitigation. *Minerals* **2022**, *12*, 136. [CrossRef]
28. Bhoi, B.; Jouhari, A.K.; Ray, H.S.; Misra, V.N. Smelting Reduction Reactions by Solid Carbon Using Induction Furnace: Foaming Behaviour and Kinetics of FeO Reduction in CaO–SiO₂–FeO Slag. *Ironmak. Steelmak.* **2006**, *33*, 245–252. [CrossRef]
29. Ru, B.; Wang, S.; Dai, G.; Zhang, L. Effect of Torrefaction on Biomass Physicochemical Characteristics and the Resulting Pyrolysis Behavior. *Energy Fuels* **2015**, *29*, 5865–5874. [CrossRef]
30. Sahajwalla, V.; Zaharia, M.; Kongkarat, S.; Khanna, R.; Rahman, M.; Saha-Chaudhury, N.; O'Kane, P.; Dicker, J.; Skidmore, C.; Knights, D. Recycling End-of-Life Polymers in an Electric Arc Furnace Steelmaking Process: Fundamentals of Polymer Reactions with Slag and Metal. *Energy Fuels* **2012**, *26*, 58–66. [CrossRef]
31. Zheng, Y.; Zhai, C.; Chen, A.; Yu, X.; Xu, J.; Sun, Y.; Cong, Y.; Tang, W.; Zhu, X.; Li, Y. Microstructure Evolution of Bituminite and Anthracite Modified by Different Fracturing Fluids. *Energy* **2023**, *263*, 125732. [CrossRef]
32. Koveria, A.; Kieush, L.; Svietskina, O.; Perkov, Y. Metallurgical Coke Production with Biomass Additives. Part 1. A Review of Existing Practices. *Can. Metall. Q.* **2020**, *59*, 417–429. [CrossRef]
33. Kieush, L.; Schenk, J.; Pfeiffer, A.; Koveria, A.; Rantitsch, G.; Hopfinger, H. Investigation on the Influence of Wood Pellets on the Reactivity of Coke with CO₂ and Its Microstructure Properties. *Fuel* **2022**, *309*, 122151. [CrossRef]
34. Bazaluk, O.; Kieush, L.; Koveria, A.; Schenk, J.; Pfeiffer, A.; Zheng, H.; Lozynskyi, V. Metallurgical Coke Production with Biomass Additives: Study of Biocoke Properties for Blast Furnace and Submerged Arc Furnace Purposes. *Materials* **2022**, *15*, 1147. [CrossRef]
35. Norgate, T.; Haque, N.; Somerville, M.; Jahanshahi, S. Biomass as a Source of Renewable Carbon for Iron and Steelmaking. *ISIJ Int.* **2012**, *52*, 1472–1481. [CrossRef]
36. Yunos, N.F.M.; Zaharia, M.; Idris, M.A.; Nath, D.; Khanna, R.; Sahajwalla, V. Recycling Agricultural Waste from Palm Shells during Electric Arc Furnace Steelmaking. *Energy Fuels* **2012**, *26*, 278–286. [CrossRef]
37. Nwachukwu, C.M.; Wang, C.; Wetterlund, E. Exploring the Role of Forest Biomass in Abating Fossil CO₂ Emissions in the Iron and Steel Industry—The Case of Sweden. *Appl. Energy* **2021**, *288*, 116558. [CrossRef]

38. Toktarova, A.; Karlsson, I.; Rootzén, J.; Göransson, L.; Odenberger, M.; Johnsson, F. Pathways for Low-Carbon Transition of the Steel Industry—A Swedish Case Study. *Energies* **2020**, *13*, 3840. [[CrossRef](#)]
39. Shukla, I. Potential of Renewable Agricultural Wastes in the Smart and Sustainable Steelmaking Process. *J. Clean. Prod.* **2022**, *370*, 133422. [[CrossRef](#)]
40. Bianco, L.; Baracchini, G.; Cirilli, F.; Moriconi, A.; Moriconi, E.; Marcos, M.; Demus, T.; Echterhof, T.; Pfeifer, H.; Beiler, C. *Sustainable EAF Steel Production (GREENEAF)*; Publications Office of the European Union: Luxembourg, 2013.
41. Fidalgo, B.; Berruoco, C.; Millan, M. Chars from Agricultural Wastes as Greener Fuels for Electric Arc Furnaces. *J. Anal. Appl. Pyrolysis* **2015**, *113*, 274–280. [[CrossRef](#)]
42. Kalde, A.; Demus, T.; Echterhof, T.; Pfeifer, H. Determining the Reactivity of Biochar-Agglomerates to Replace Fossil Coal in Electric Arc Furnace Steelmaking. In Proceedings of the EUBCE 2015 Online Conference Proceedings, Vienna, Austria, 1–4 June 2015; pp. 497–507.
43. Huang, X.-A.; Ng, K.W.; Giroux, L.; Duchesne, M. Carbonaceous Material Properties and Their Interactions with Slag during Electric Arc Furnace Steelmaking. *Met. Mater. Trans. B* **2019**, *50*, 1387–1398. [[CrossRef](#)]
44. *ASTM D3172-13*; Standard Practice for Proximate Analysis of Coal and Coke. ASTM International: West Conshohocken, PA, USA, 2013.
45. *ISO 18125:2017*; Solid Biofuels—Determination of Calorific Value. International Organization for Standardization: Geneva, Switzerland, 2017.
46. *ISO 1928:2020*; Coal and Coke—Determination of Gross Calorific Value. International Organization for Standardization: Geneva, Switzerland, 2020.
47. *ISO 18894:2018*; Coke—Determination of Coke Reactivity Index (CRI) and Coke Strength after Reaction (CSR). International Organization for Standardization: Geneva, Switzerland, 2018.
48. *ISO 9277:2010*; Determination of the Specific Surface Area of Solids by Gas Adsorption—BET Method. International Organization for Standardization: Geneva, Switzerland, 2010.
49. Warren, B.E. X-ray Diffraction in Random Layer Lattices. *Phys. Rev.* **1941**, *59*, 693–698. [[CrossRef](#)]
50. Okolo, G.N.; Neomagus, H.W.J.P.; Everson, R.C.; Roberts, M.J.; Bunt, J.R.; Sakurovs, R.; Mathews, J.P. Chemical-Structural Properties of South African Bituminous Coals: Insights from Wide Angle XRD–Carbon Fraction Analysis, ATR–FTIR, Solid State ¹³C NMR, and HRTEM Techniques. *Fuel* **2015**, *158*, 779–792. [[CrossRef](#)]
51. Li, J.; Xu, R.; Wang, G.; Zhang, J.; Song, B.; Liang, W.; Wang, C. Study on the Feasibility and Co-Combustion Mechanism of Mixed Injection of Biomass Hydrochar and Anthracite in Blast Furnace. *Fuel* **2021**, *304*, 121465. [[CrossRef](#)]
52. Rantitsch, G.; Bhattacharyya, A.; Günbati, A.; Schulten, M.-A.; Schenk, J.; Letofsky-Papst, I.; Albering, J. Microstructural Evolution of Metallurgical Coke: Evidence from Raman Spectroscopy. *Int. J. Coal Geol.* **2020**, *227*, 103546. [[CrossRef](#)]
53. *ASTM D4326-21*; Standard Test Method for Major and Minor Elements in Coal Ash By X-ray Fluorescence. ASTM International: West Conshohocken, PA, USA, 2021.
54. Shamsudin, R.; Abdul Azam, F.A.; Abdul Hamid, M.; Ismail, H. Bioactivity and Cell Compatibility of β -Wollastonite Derived from Rice Husk Ash and Limestone. *Materials* **2017**, *10*, 1188. [[CrossRef](#)] [[PubMed](#)]
55. Lünsdorf, N.K.; Dunkl, I.; Schmidt, B.C.; Rantitsch, G.; von Eynatten, H. Towards a Higher Comparability of Geothermometric Data Obtained by Raman Spectroscopy of Carbonaceous Material. Part 2: A Revised Geothermometer. *Geostand. Geoanal. Res.* **2017**, *41*, 593–612. [[CrossRef](#)]
56. European Commission. *Directorate General for Research and Innovation. Flexible Production of Coke Using Alternative Coals: Effects on Coke Properties under Blast Furnace Conditions (FLEXCOKE): Final Report*; Publications Office: Luxembourg, 2019.
57. Hilding, T.; Gupta, S.; Sahajwalla, V.; Björkman, B.; Wikström, J.-O. Degradation Behaviour of a High CSR Coke in an Experimental Blast Furnace: Effect of Carbon Structure and Alkali Reactions. *ISIJ Int.* **2005**, *45*, 1041–1050. [[CrossRef](#)]
58. El-Tawil, A.A.; Björkman, B.; Lundgren, M.; Bäck, F.; Ökvist, L.S. Influence of Modified Bio-Coals on Carbonization and Bio-Coke Reactivity. *Metals* **2021**, *12*, 61. [[CrossRef](#)]
59. Dun, W.; Gujian, L.; Ruoyu, S.; Xiang, F. Investigation of Structural Characteristics of Thermally Metamorphosed Coal by FTIR Spectroscopy and X-ray Diffraction. *Energy Fuels* **2013**, *27*, 5823–5830. [[CrossRef](#)]
60. Wang, M.; Wei, G.; Zhu, R.; Dong, K. Effect of CO₂-O₂ Oxidizing Atmospheres on the Combustion Characteristics of Metallurgical Coke and Anthracite. *J. CO₂ Util.* **2021**, *52*, 101665. [[CrossRef](#)]
61. Ng, K.W.; MacPhee, J.A.; Giroux, L.; Todoschuk, T. Reactivity of Bio-Coke with CO₂. *Fuel Process. Technol.* **2011**, *92*, 801–804. [[CrossRef](#)]

Disclaimer/Publisher’s Note: The statements, opinions and data contained in all publications are solely those of the individual author(s) and contributor(s) and not of MDPI and/or the editor(s). MDPI and/or the editor(s) disclaim responsibility for any injury to people or property resulting from any ideas, methods, instructions or products referred to in the content.